remote sensing

MDPI

Article

Evaluation of Himawari-8/AHI, MERRA-2, and CAMS Aerosol Products over China

Taixin Zhang [1], Lin Zang [2,*], Feiyue Mao [1], Youchuan Wan [1] and Yannian Zhu [3]

[1] School of Remote Sensing and Information Engineering, Wuhan University, Wuhan 430079, China; rsztx@whu.edu.cn (T.Z.); maofeiyue@whu.edu.cn (F.M.); ychwan@whu.edu.cn (Y.W.)
[2] Chinese Antarctic Centre of Surveying and Mapping, Wuhan University, Wuhan 430079, China
[3] Meteorological Institute of Shaanxi Province, Xi'an 710014, China; yannianzhu@gmail.com
* Correspondence: zanglin2018@whu.edu.cn; Tel.: +86-132-9654-5865

Received: 11 March 2020; Accepted: 18 May 2020; Published: 25 May 2020

Abstract: Reliable aerosol optical depth (AOD) data with high spatial and temporal resolutions are needed for research on air pollution in China. AOD products from the Advanced Himawari Imager (AHI) onboard the geostationary Himawari-8 satellite and reanalysis datasets make it possible to capture diurnal variations of aerosol loadings. However, due to the different retrieval methods, their applicability may vary with different space and time. Thus, in this study, taking the measured AOD at the Aerosol Robotic NETwork (AERONET) stations as the gold standard, the performance of the latest AHI hourly AOD product (i.e., L3 AOD) was evaluated and then compared with that of two reanalysis AOD datasets offered by Modern-Era Retrospective Analysis for Research and Applications, Version 2 (MERRA-2) and Copernicus Atmosphere Monitoring Service (CAMS), respectively, covering from July 2015 to December 2017 over China. For all the matchups, AHI AOD shows the highest robustness with a high correlation (R) of 0.82, low root-mean-square error (RMSE) of 0.23, and moderate mean absolute relative error (MARE) of 0.56. Although MERRA-2 and CAMS products both have lower R values (0.74, 0.72) and higher RMSE (0.28, 0.26), the former is slightly better than the latter. Accuracy of AOD products could be mainly affected by the pollution level and less affected by particle size distribution. Comparisons among these AOD products imply that AHI AOD is more reliable in regions with high pollution levels, such as central and eastern China, while in the northern and western part, MERRA-2 AOD seems more satisfying. The performance of all the three AOD products presents a significant diurnal variety, as indicated by the highest accuracy in the morning for AHI and at noon for reanalysis data. Moreover, due to various pollution distribution patterns and meteorological conditions, there are distinct seasonal characteristics in the performance of AOD products for different regions.

Keywords: AOD; CAMS; evaluation; Himawari-8; MERRA-2

1. Introduction

Atmospheric aerosols play an important role in the climate system by scattering and absorbing solar radiation, and also have a severely adverse influence on human health [1–3]. To understand the aerosol distribution, aerosol optical depth (AOD), retrieved from observations and model predictions, has been widely used. With the development of remote sensing technique, several satellite-based AOD products have been released and used in various applications [4,5]. However, most products, such as the Moderate Resolution Imaging Spectroradiometer (MODIS) AOD, are derived from polar-orbiting satellites, and are limited in use due to once a day observation. Recently, some products with high temporal and spatial resolutions from geostationary-orbit satellites have been available and make it possible to capture the detailed diurnal evolution of aerosols [6].

Himawari-8, a new geostationary meteorological satellite developed by the Japan Meteorological Agency (JMA), was launched on 7 October 2014 [7]. The Advanced Himawari Imager (AHI) on board it can be used to derive AOD in 10 min intervals over the East Asia-Pacific Ocean area, which covers almost the whole of China except for the parts of Xinjiang and Tibet. Some works have been conducted to evaluate the accuracy of AHI AOD over China. Zhang et al. [8] explored the performance of AHI L2 version 2 aerosol datasets by comparing with measurements in 16 ground stations over China and achieved a high coefficient of determination (R^2) of 0.67 during the period from January 2016 to December 2016. The accuracy shows dependency on seasons and land surface cover. The accuracy of AHI AOD product was also found to be varied in different regions and affected by aerosol types [9]. Therefore, despite the effectiveness of AHI AOD in monitoring aerosol distributions at a fine temporal resolution, it is essential to further consider its usability under different conditions. Furthermore, AOD is not retrievable by satellites due to cloud cover. By contrast, reanalysis AOD products show the remarkable advantages of spatio-temporal continuity.

In the past years, several institutes have produced and released reanalysis aerosol products, such as the Modern-Era Retrospective Analysis for Research and Applications Aerosol Reanalysis (MERRAero) covering the period from January 2002 to February 2012 provided by the National Aeronautics and Space Administration (NASA) Global Modeling and Assimilation Office [10], the Navy Aerosol Analysis and Prediction System aerosol reanalysis product covering the years of 2003–2015 developed by US Naval Research Laboratory [11], and the reanalysis of earlier Monitoring Atmospheric Composition and Climate (MACC) project covering the years of 2003–2012 [12]. Up to now, both MERRAero and MACC have been updated to their second generation, named as MERRA-2 and CAMS (operated in the Copernicus Atmosphere Monitoring Service), covering the period of 1980-present and 2003–2017, respectively [13,14]. Among all the reanalysis aerosol products, MERRA-2 and CAMS cover a longer time period, and they can be used in the air pollution research of the most recent time. Shi et al. [15] evaluated the MODIS and MERRAero/MERRA-2 AOD products based on 400 Aerosol Robotic NETwork (AERONET) sites over the world from 2002 to 2015, and results show that MERRA-2 AOD dataset has comparable accuracy with the MODIS AOD dataset at the low AOD value region, while under severe haze conditions in China, MERRA-2 has a notable bias, which may be attributed to the systemic bias of the assimilation system [16]. The performance of the MACC reanalysis aerosol dataset also showed a larger bias in some regions and seasons [12]. These works indicated that reanalysis data could be inaccurate due to various issues, including limitations in model physics, resolution, and the underlying sources used for assimilation. Therefore, the reanalysis AOD datasets need to be verified and intercompared before using them.

In recent years, aerosol pollution in China elicits considerable public concern, especially in the central and eastern regions [17]. It is significant and necessary to capture the aerosol distributions at a fine spatio-temporal resolution. Though Himawari-8/AHI and reanalysis AOD products can characterize the diurnal variations of aerosols, there may be some limitations in different times and areas due to their different mechanisms in obtaining AOD. In this work, we evaluated and compared the performance of AOD products from AHI, MERRA-2, and CAMS over China against ground-based observations from AERONET. The influence of pollution levels and particle size distribution on AOD performance was also considered. Related results could provide guidance for better usage of various AOD products in China.

2. Data and Method

2.1. Himawari-8 AOD

As a geostationary satellite, Himawari-8 covers the range of 80° E–160° W and 60° N–60° S. The AHI on board is a state-of-the-art sensor, and it conducts a full-disk observation every 10 min. The sensor has 16 bands, including 6 wavelengths from the visible to near-infrared, which are well-configured for the retrieval of aerosol properties [18]. Based on an assumed aerosol model, surface

reflectance model, and cloud detection algorithm, L2 AOD ($AOD_{original}$) products can be retrieved following the algorithm described in Daisaku [6]. Then an hourly-combined algorithm is applied to retrieve another two datasets of L3 products: AOD_{pure} and AOD_{merged}. AOD_{pure} is an extracted set of the $AOD_{original}$ (L2 AOD) with strict cloud screenings. It would be assigned a missing value if a cloudy pixel existed within 12.5 km, or the number of effective pixels was below 20% of the total possible number of observations within a distance of 12.5 km and 1 h. Furthermore, AOD_{merged} is calculated by the optimum interpolation of the AOD_{pure} within the radius of 12.5 km and past 1 h. In general, the two hourly AODs are derived using the variability information taking into account the difference and distance of the past and surrounding pixels from the point of interest [19]. Until now, L3 hourly AOD has been published for three versions, i.e., 010, 020 (and interim version) and 030. Major updates in version 030 are carried out based on the aerosol models established by Omar et al. [20] and Sayer et al. [21], as well as surface reflectance from Fukuda et al. [22].

Overall, L3 AOD provides three types of datasets, i.e., the original, pure, and merged. Considering AOD_{merged} can give a maximum number of aerosol retrievals and better performance compared with AOD_{pure} and $AOD_{original}$ [19], we only focus on the AOD_{merged} dataset and compare it with reanalysis datasets from MERRA-2 and CAMS. Notably, only the highest-level retrievals labeled with 'very good' were used in this work.

2.2. MERRA-2 and CAMS AOD

As the MERRA data assimilation system is not able to ingest new observations, it has been replaced by MERRA-2 reanalysis. The MERRA-2 uses the upgraded Goddard Earth Observating System, Version 5 (GEOS-5) modeling system, which is radiatively coupled to the Goddard Chemistry, Aerosol, Radiation, and Transport (GOCART) model, to simulate aerosols [13]. Aerosols in GOCART are represented by 15 tracers (bins), consisting of five size bins spanning 0.03–10 μm for sea salt, 0.1–10 μm for dust, hydrophobic and hydrophilic black and organic carbon, and sulfate (SO_4). The aerosol particles are assumed externally mixed. MERRA-2 assimilated AOD observations of the Advanced Very High Resolution Radiometer (1980–August 2002), AERONET (1999–October 2014), Multi-angle Imaging SpectroRadiometer (MISR, February 2000–June 2014), MODIS Terra (March 2000 onwards), and MODIS Aqua (August 2002 onwards). MISR AOD is only assimilated over the bright land surface. Collection 5 AOD products of MODIS/Terra and MODIS/Aqua retrieved by Dark Target (DT) algorithm are used in MERRA-2 aerosols. MERRA-2 aerosol product covers the time period from 1980 to the present. The 1-hour time-averaged collections of AOD were used in this work.

The European Center for Medium-Range Weather Forecasts (ECMWF) produces CAMS reanalysis (CAMSRA) with the updated Integrated Forecast System (IFS), which uses the new version of the Carbon Bond mechanism developed in 2005 (CB05) [14,23]. The aerosol module of IFS is a bulk-bin scheme simulating five types of aerosols with 12 prognostic tracers. There are three size bins for sea salt (0.030–0.55, 0.55–0.9, 0.9–20 μm), similarly three bins for dust (0.030–0.55, 0.55–0.9, 0.9–20 μm), organic matter, and black carbon with the hydrophilic and hydrophobic component, sulfur dioxide (SO_2) and sulfate aerosol (SO_4). CAMS reanalysis assimilated satellite AODs of the Envisat Advanced Along-Track Scanning Radiometer (AATSR), MODIS/Terra, and MODIS/Aqua. The AATSR AOD is only assimilated to the dataset spanning from December 2002 to March 2012. Both MODIS/Terra and MODIS/Aqua AODs are assimilated from October 2002 onwards. Collection 6 AODs at 550 nm of MODIS were used in CAMS reanalysis. They were retrieved through the enhanced Deep Blue (DB) and DT algorithms over land, and the DT algorithm over the ocean. CAMS reanalysis covers a time period from 2003 to 2017 (last access: February 2020) with a 3-hour time resolution and will be extended in the future.

Both MERRA-2 and CAMS provide AOD datasets of multiple wavelengths. Here considering AHI AOD is obtained at 500 nm, we only used their AODs at 550 nm to be compared. The basic characteristics of the three AOD products are summarized in Table 1. As a result of the different time coverage of these AOD products, the time range of this study is from July 2015 to December 2017.

Table 1. Description of Aerosol Optical Depth (AOD) datasets.

	AERONET	AHI	MERRA-2	CAMS
Production Coverage	Worldwide	East Asia-Pacific Ocean	World wide	World Wide
Time Resolution	1 min	1 h	1 h	3 h
Spatial Resolution	Point measurement	0.05°	0.5°*0.625°	80 km
Related variables	AOD (multiple-wavelength) AE	AOD 500 nm	AOD 550 nm	AOD 550 nm
Agency	NASA	JAXA	NASA	ECMWF

2.3. AERONET Observations

AERONET is a global ground-based network, providing long-term measurements of aerosol optical properties at wide-range wavelengths from 340 to 1640 nm with a high temporal resolution [24]. Up to now, there are more than 600 sites over the world. The newest database of version 3 has been released with improved cloud screening approaches, spectral temperature characterization of the instrument, and further quality control. In this study, AODs of version 3, retrieved by the AERONET Direct Sun Algorithm, were used. Ångström exponent (AE) mentioned in the following work is obtained based on the AODs of 440 and 675 nm.

The sun-photometer (provided by the CIMEL company) equipped at AERONET sites provides AOD at 500 nm that can be used to be compared with AHI AOD directly. As for the comparison with reanalysis products, we used a second-order polynomial fitting of AERONET AODs at wavelengths in logarithmic coordinates from 340 to 1080 nm to interpolate to AOD 550 nm [25–27].

2.4. Evaluation Methods

To compare the accuracy of different datasets, it is essential to develop a proper matchup strategy. In terms of the generation of AHI L3 dataset based on the L2 original AOD information of pixels within 12.5 km and past 1 h, AODs from AHI in a 6*6 pixels window (~15 km in radius) centered the ground site were spatially averaged. Then, AERONET observations within the past 60 min of Himawari-8 measuring time were averaged as the corresponding ground-based AOD value. The reanalysis aerosol datasets used in this work are time-averaged, therefore they can be used directly by searching for the nearest-neighbor data to the site. All AOD datasets are matched synchronously to eliminate temporal heterogeneities when comparing the performance of different products. Each AOD product is individually evaluated based on AERONET dataset and then compared with each other.

By matching all the datasets, there are only 18 sites that have over 50 matchups during the period from July 2015 to December 2017. They can be used in indicating AOD performance in different regions. As shown in Figure 1, except for Baotou, Taihu, and Hong Kong (HK) sites, which were located in Inner Mongolia, Taihu Lake, and Hong Kong, respectively. The other 15 sites were grouped into two categories based on their geophysical locations. Specifically, nine sites labeled 1 and 3–10 are divided into the North China Plain (NCP) and six sites labeled 12–17 into Taiwan (TW) regions, respectively.

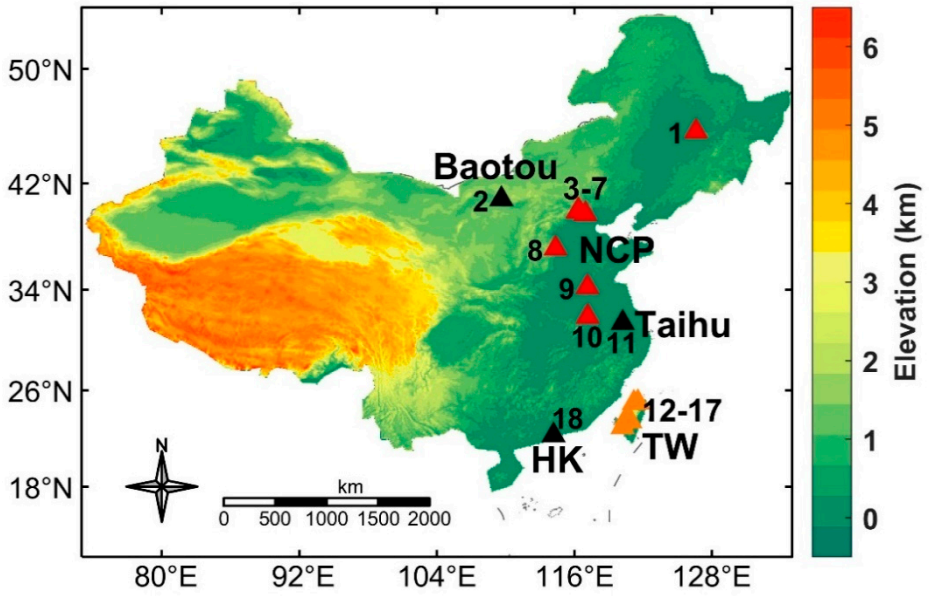

Figure 1. Distribution of the Aerosol Robotic NETwork (AERONET) sites in China. Red sites labeled with 1 and 3–10 are grouped into the North China Plain (NCP) region, orange sites of 12–17 into the Taiwan (TW) region. Three black sites (2, 11, 18) are named as Baotou, Taihu, and Hong Kong (HK), respectively. Color-bar represents the elevations from the digital elevation model provided by the Shuttle Radar Topographic Mission of National Aeronautics and Space Administration.

We applied the following parameters to evaluate AOD product performance: (1) correlation coefficient (R), representing the degree of correlation between two AOD datasets; (2) root-mean-square error (RMSE), referring to the standard deviation of the bias between AOD from AHI/reanalysis and AERONET (true value); (3) mean absolute relative error (MARE), dividing the mean absolute bias of two AOD datasets by true value. RMSE and MARE were described by Equations (1) and (2):

$$\mathrm{RMSE} = \sqrt{\frac{1}{n}\sum_{1}^{n}\left(\mathrm{AOD}^{i} - \mathrm{AOD}^{i}_{\mathrm{AERONET}}\right)^{2}}, \tag{1}$$

$$\mathrm{MARE} = \frac{1}{n}\sum_{1}^{n}\left|\frac{\mathrm{AOD}^{i} - \mathrm{AOD}^{i}_{\mathrm{AERONET}}}{\mathrm{AOD}^{i}_{\mathrm{AERONET}}}\right| \tag{2}$$

Apart from these three statistical parameters, an orthogonal linear regression (OLR) method was used to derive the regression lines for the AOD datasets against ground-based observations, which accounts for uncertainties in both the dependent and independent variables [28,29]. The OLR method minimizes the orthogonal distance (other than the vertical distance in ordinary least square regression) between the regression line and each data point, as denoted by Equation (3):

$$S = \sqrt{\sum_{i=1}^{N}\left[\left(x_i - X_i\right)^2 + \left(y_i - Y_i\right)^2\right]}, \tag{3}$$

where $[x_i, y_i]$ and $[X_i, Y_i]$ are observed and regressed points, respectively.

3. Results and Discussion

3.1. Comparisons for all Pollution Levels

The AHI L3 AOD product has been upgraded from version 010 (V010) to 030 (V030), and both of them have three datasets of $AOD_{original}$, AOD_{pure}, and AOD_{merged}, covering the most recent observation time. Here we evaluated the two AOD_{merged} products from version 010 and 030 based on in-situ observations from AERONET, as shown in Figure 2a,b. There are 12,238 high-quality matchups from July 2015 to December 2017. The AHI V030 dataset has a good agreement with ground-based observations with a correlation coefficient of 0.82, RMSE of 0.23, and MARE of 0.56. While V010 AOD performance is not satisfactory as V030, indicated by a higher RMSE (0.27) and MARE (0.61). What is more, the steeper slope of the OLR regression line for the AHI V030 dataset demonstrates a significant improvement in the problem of underestimation at high AOD. Thus, in the following work, we only focus on the AHI AOD_{merged} dataset from the 030 version.

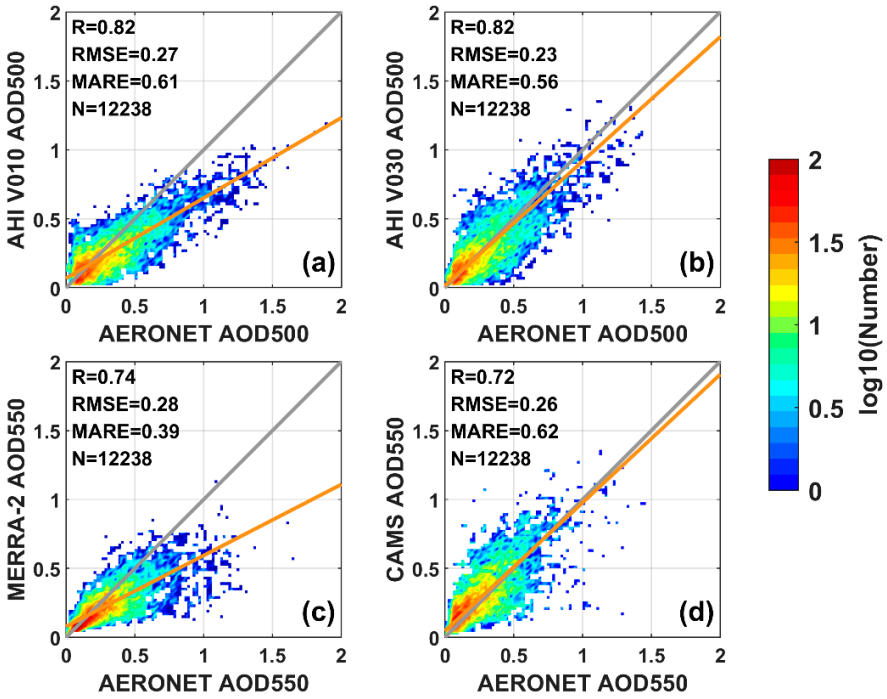

Figure 2. Scatterplots of aerosol optical depths (AOD) from the (**a**) Advanced Himawari Imager (AHI) version 010 (V010), (**b**) AHI V030, (**c**) Modern-Era Retrospective Analysis for Research and Applications, version 2 (MERRA-2), and (**d**) Copernicus Atmosphere Monitoring Service (CAMS) versus AERONET observations. The grey line and orange line refer to the one-to-one line and linear-regression line, respectively. The parameter N is the number of matchups; R, RMSE, and MARE represent the correlation coefficient, the root-mean-square error, and the mean absolute relative error, respectively. Color-bar represents the logarithm of matchup numbers for a corresponding pixel.

Validation results of AODs from MERRA-2 and CAMS are presented in Figure 2c,d. A comparison between the two reanalysis products shows that MERRA-2 has a higher R and lower MARE value than CAMS. However, opposite to AHI datasets, both of them demonstrate a weaker correlation with ground-based observations. Their slopes of linear-regression lines, especially MERRA-2, are much lower than the one-to-one lines with high aerosol loadings, indicating the significant underestimation of AOD. Referred to the mechanism of modeling system, both aerosol modules of MERRA-2 and CAMS simulate five aerosol types, i.e., dust, sea salt, black carbon, organic carbon (organic matter in CAMS), and sulfate aerosols, while nitrate aerosols are not included [13,16,30], which might be

mostly responsible for the underestimation of reanalysis AODs, especially in regions with a large mass fraction of nitrate [31].

Further investigation was conducted to evaluate the performance of AHI and reanalysis AOD products in different regions, as shown in Figure 3. The scatterplots of AODs from AHI, MERRA-2, and CAMS versus AERONET observations imply the much better performance of AHI AOD than reanalysis AODs in the regions of NCP, HK, TW, and Taihu, except for Baotou. Comparatively, MERRA-2 AOD performs best in Baotou with the highest R value (0.77), lowest RMSE (0.07), and MARE (0.37). According to previous literature, the accuracy of satellite-based aerosol retrieval is limited in regions covered by bright surfaces because of the increased uncertainty of surface reflectance [32,33], which largely explains the poor performance of AHI AOD in Baotou, situated in bare land. In addition, AHI tends to underestimate AOD in HK and TW, as indicated by the lower linear-regression line slopes. In the generation of AHI AOD, the surface reflectance is combined from clear sky observations within one month. In the rainy weather of the tropics, it is relatively difficult to obtain effective surface reflectance, which could be overestimated on wet ground (different from the dry surface) and result in an underestimation of AOD. In addition, under high humidity, the moisture absorption growth of hydrophilic aerosols such as sea-salt aerosols will enlarge the extinction efficiency of aerosols, especially near the surface, thus increasing the bias between ground-based AOD and satellite-retrieved AOD [34].

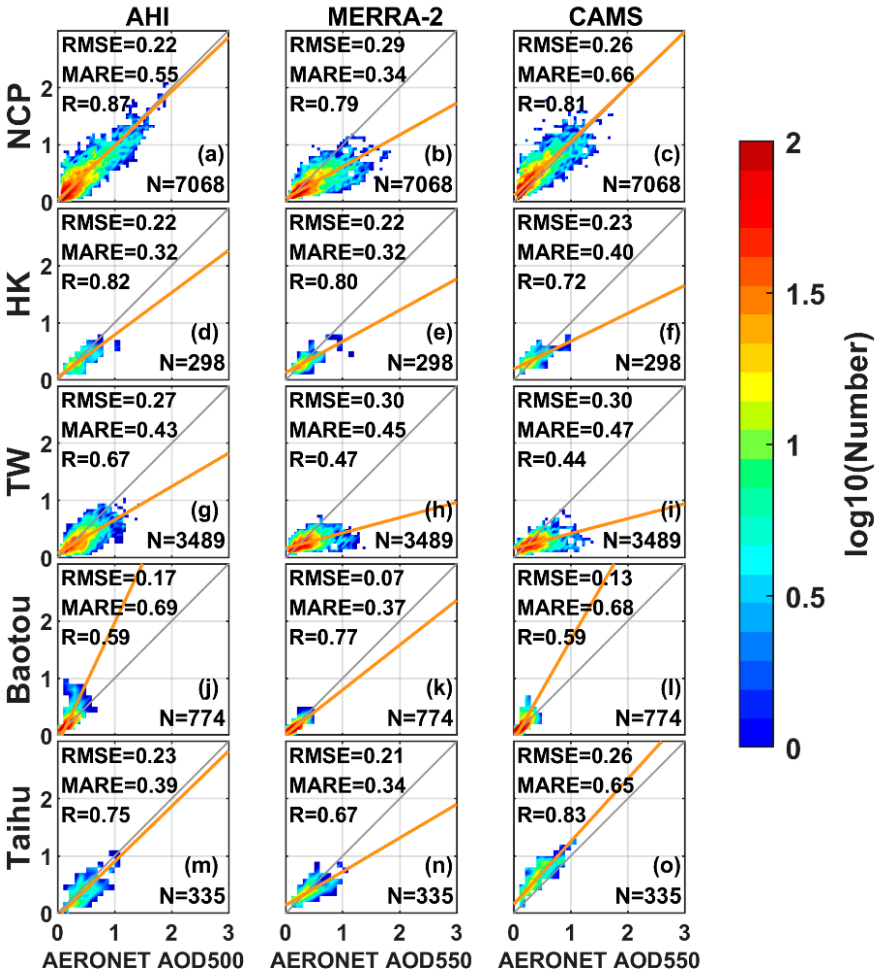

Figure 3. Scatterplots of AODs from AHI, MERRA-2, and CAMS versus AERONET observations in the (**a**–**c**) NCP, (**d**–**f**) HK, (**g**–**i**) TW, (**j**–**l**) Baotou, and (**m**–**o**) Taihu regions. The y-axis of columns 1–3 indicates AODs from AHI, MERRA-2, and CAMS, respectively.

To investigate the impact of heterogeneity in land surface cover on the accuracy of AOD products, we conducted a research based on matchups centered by pixels with large variations of land surface cover around. Considering that some ground sites are located near water, there might be some pixels surrounding a site that are water covered. AHI AOD is retrieved based on different bands and aerosol model setting, and it might decrease the accuracy of averaged values when the ocean covered pixels are included in the sample window. We searched all the grid cells centered on each ground site within a window of 0.15°*0.15°. If any grid is covered by water, this site is considered as a near-water site. Three sites (Chen_Kung_Univ, Chiay, EPA_NCU) in TW, as well as Taihu and Hong_Kong_PolyU sites, are found to be near-water sites.

Figure 4a–d represents the accuracy of AHI AOD datasets in Chen_kung_Univ and EPA_NCU with full matchups and selected matchups only including land pixels, respectively. The selected matchups in column 2 were obtained by excluding near-water pixels in the matching windows. Though the regression lines of AHI AOD are closer to the one-to-one lines in Chen_Kung_Univ and EPA_NCU when near-water pixels are excluded, there are no remarkable improvements in RMSE and MARE. In the meantime, reanalysis AOD datasets perform worse in EPA_NCU, as shown in Figure 4e–f. In addition, it should also be noted the number of matchups has lost a lot. Therefore, there are no significant advantages to exclude water-covered pixels.

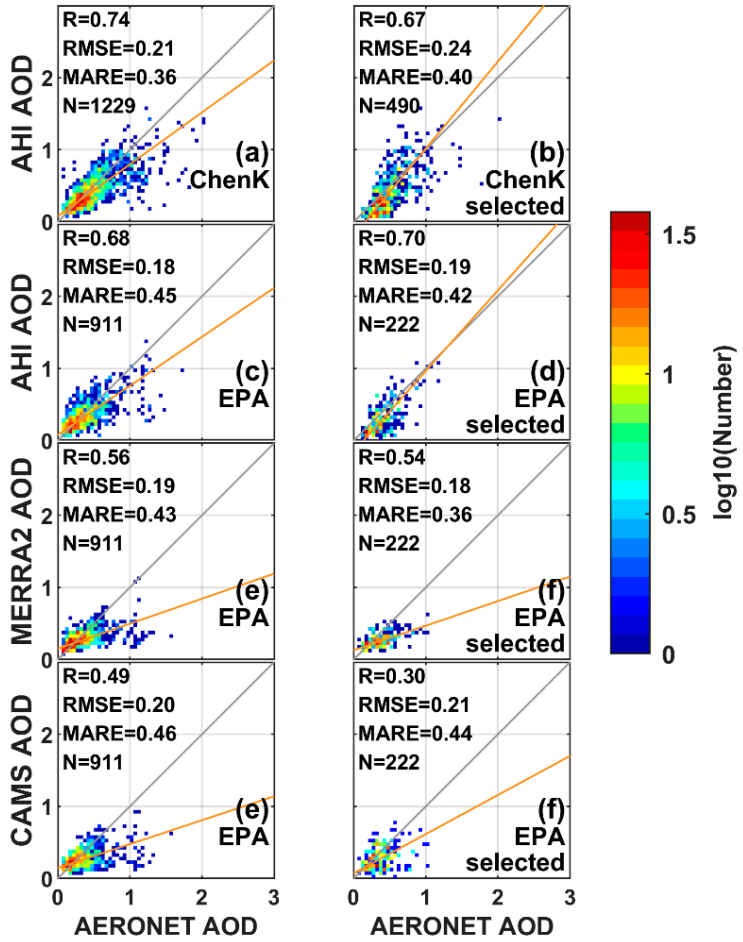

Figure 4. Scatterplots of AHI, MERRA-2, and CAMS AOD versus AERONET AOD in Chen_Kung_Univ and EPA_NCU sites; (**a**–**d**) represents the accuracy of AHI AOD datasets in Chen_kung_Univ and EPA_NCU with full matchups and selected matchups only including land pixels, (**e**–**f**) reanalysis AOD datasets. Columns 1 and 2 indicate the evaluation results of matchups with near-water pixels involved and excluded, respectively.

3.2. Comparisons Under Different Pollution Levels

To further understand the effects of pollution levels on the AOD product performance in different regions, additional validation was carried out, as shown in Figure 5. Here, AOD matchups in each sub-region (i.e., the NCP, HK, TW, and Taihu) were divided into two groups, i.e., AOD (measured by AERONET) > 0.5 and ≤ 0.5. Very few AOD retrievals are higher than 0.5 in Baotou, therefore there is no need to validate the datasets in high AOD values in this region. As illustrated in the first column of Figure 5, the regression lines of AHI AOD are much closer to the one-to-one lines when AOD > 0.5 in NCP, HK, and Taihu, and there are much higher R and lower MARE values. This could be ascribed to the higher signal-to-noise ratio and less sub-pixel cloud contamination under polluted levels [15,35,36]. MARE of AHI AOD is also reduced when AOD > 0.5 in TW. Notably, compared with MERRA-2 and CAMS, AHI has the best accuracy with the highest R (0.8, 0.74, 0.42) and lowest MARE (0.24, 0.29, 0.37) in NCP, HK, and TW when AOD > 0.5. However, when AOD ≤ 0.5, AHI shows relatively poor performance in all areas, and MERRA-2 demonstrates the high reliability in NCP and HK. In the TW region, the two reanalysis products have comparable performance.

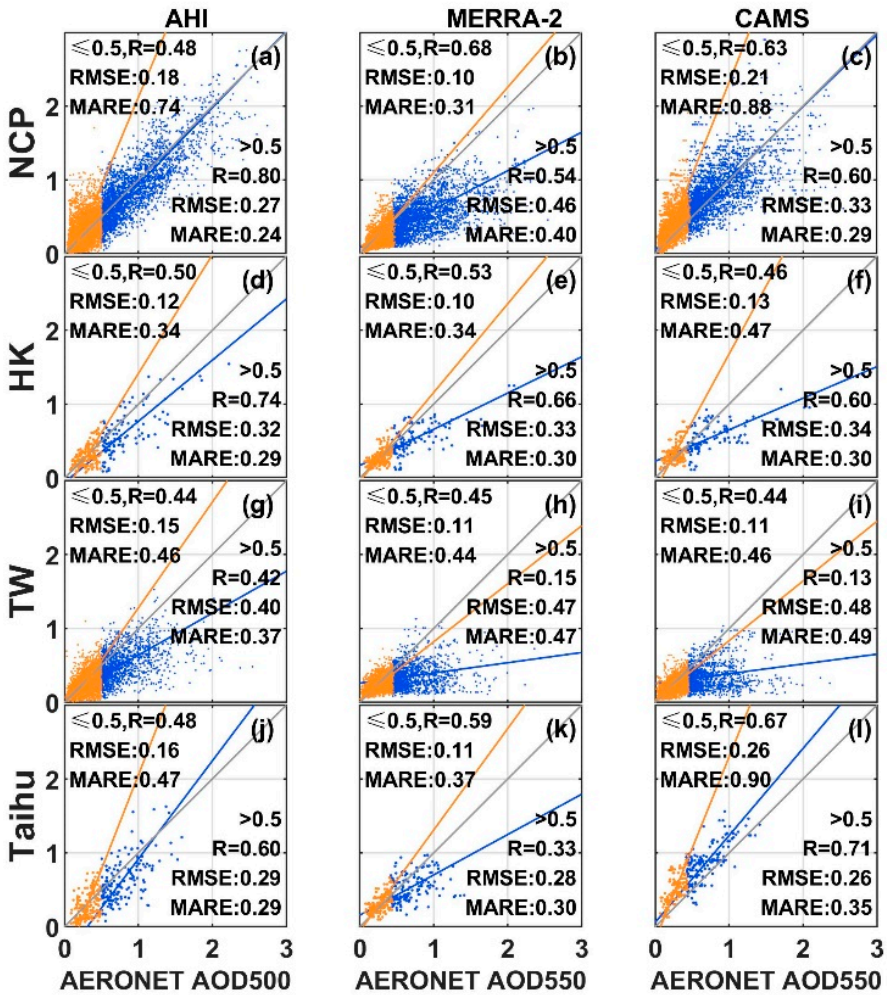

Figure 5. Scatterplots of AODs from AHI, MERRA-2, and CAMS versus AERONET observations in the (**a**–**c**) NCP, (**d**–**f**) HK, (**g**–**i**) TW, and (**j**–**l**) Taihu regions when AOD > 0.5 (in blue) and ≤0.5 (in orange), respectively. The y-axis of columns 1–3 indicates AODs from AHI, MERRA-2, and CAMS, respectively.

AOD retrievals highly rely on the adopted aerosol model; thus, the accuracy would be affected by the type assumption of aerosol particles [19]. AE is an indicator of the aerosol particle size, which is important for identifying aerosol types or sources. Generally, small AE indicates large particles like dust

aerosols, while large AE indicates fine particles mainly from anthropogenic aerosols [37]; and AE < 1 has been considered as a typical aerosol size distribution dominated by coarse mode [38,39]. In this work, a further comparison was conducted to evaluate the AOD performance of the three datasets for two AE categories (AE > 1 V.S. AE ≤ 1), as shown in Figure 6. The AE values were obtained at the wavelength of 440–675 nm from AERONET observations. When AE > 1, it is apparent that there are much lower MARE and better regression lines (closer to the one-to-one line) of AHI AOD in the four regions, as shown in the first column of Figure 6. However, there is no apparent regularity about the accuracy of the reanalysis AODs. Taken together the statistical parameters with the regression line, the performance of AHI AOD is better than that of MERRA-2 and CAMS AODs in NCP, TW, and Taihu on the condition of AE > 1. It should be noted that MERRA-2 shows the absolute advantages in Baotou among the three products, both in AE > 1 and ≤ 1.

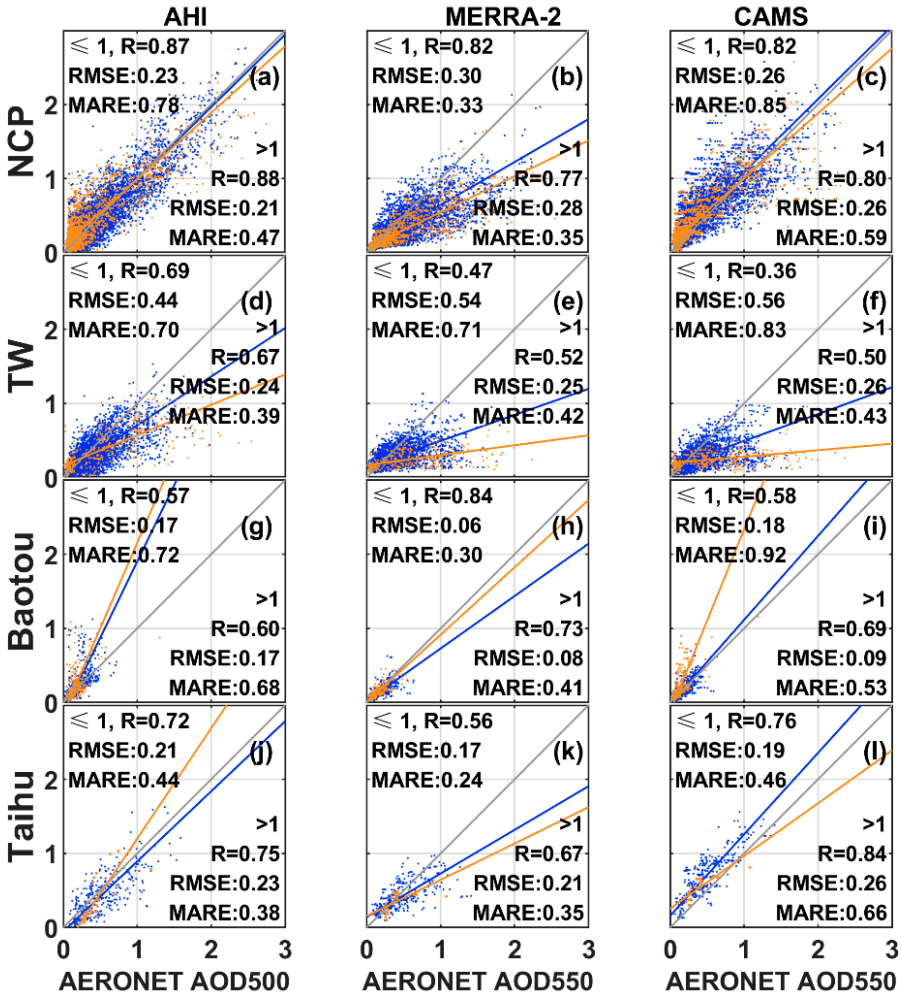

Figure 6. Scatterplots of AHI, MERRA-2, and CAMS AOD versus AERONET AOD in NCP, HK, and TW when AE > 1 (in orange) and ≤1 (in blue), respectively (**a**–**l**). The y-axis of columns 1–3 indicates AODs from AHI, MERRA-2, and CAMS, respectively.

In general, the performance of AHI AOD can be improved under the condition of higher pollution levels or with a larger fraction of fine particles. However, satellite retrieved AOD can be less accurate over the bright surface, like bare land in Baotou, due to the low signal-to-noise ratio as a result of high surface reflectivity. The reanalysis products underestimate AOD in any pollution levels and particle size distributions in TW. There are up to 26.4% sea-salt aerosols contributing to the total AOD on the annual average in TW [40]. However, quantifications of sea-salt aerosol are still not satisfied with a larger uncertainty than that of other aerosols [41]. On the one hand, hygroscopic

growth of sea-salt particles might affect the accuracy of AOD retrievals. On the other hand, sea salt is represented by bins spanning 0.03–10 μm dry radius in the GOCART module and 0.03–20 μm radius at 80 % relative humidity in the IFS system, assuming that coarse mode sea salt settles quickly after emitted. While strong wind accompanied by vertical velocity can transport coarse particles into the boundary layer [42], as a result, modeled sea-salt aerosol might be underestimated. In addition, the overestimation of surface reflectance is another factor of AOD underestimation.

3.3. Diurnal and Seasonal Comparisons

The three datasets discussed in previous sections can be used to capture the sub-daily variations of AOD. Comparisons of AOD performance among these products at different times are necessary. Figure 7 displays the diurnal variations of R, RMSE, and MARE from AHI, MERRA-2, and CAMS AOD versus AERONET observations from 08:00 to 17:00 local time (LT). AHI shows the best accuracy in the morning with a higher correlation, lower RMSE, and MARE. The possible explanation is the high AOD levels in the morning, which might be contributed by significant emissions [43,44]. There are larger MARE values during the time period from 13:00 to 15:00, which might be ascribed to the lower AOD. Interestingly, MERRA-2 AOD shows better performance with the highest R and moderate RMSE (MARE) at noon. The main reason can be supported by prior studies that MODIS AOD retrievals from Aqua (afternoon satellite) outperform Terra (morning satellite), both of which have been assimilated into reanalysis aerosol products [45,46]. In addition, the relative humidity near the surface has a significant decrease at noon, and meantime the boundary layer height is lifted [47]. Both changes benefit the estimation of AOD by reducing the effect of hygroscopic growth and making the particles mixed well. Overall, AHI AOD performs better than MERRA-2 and CAMS during the daytime in terms of the significant lower R and RMSE values.

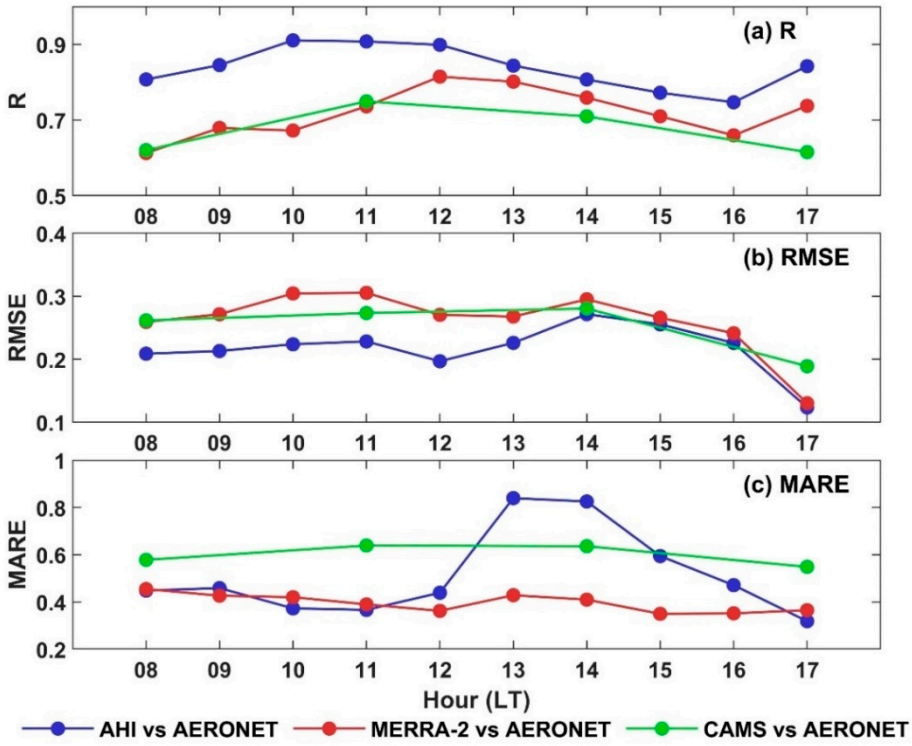

Figure 7. Diurnal variations of (**a**) R, (**b**) RMSE, and (**c**) MARE from AHI (blue), MERRA-2 (red), and CAMS (green) AOD versus AERONET observations from 08:00 to 17:00 local time (LT).

The seasonal accuracy of AOD datasets was explored in the NCP and TW regions because of their great differences in geo-locations and climate patterns. As indicated in the previous sections, the accuracy of AODs is significantly impacted by pollution levels, and also can be decreased by the

water-uptake effect of aerosols under humid conditions. Figure 8 presents the validation statistics of AHI and reanalysis AODs versus ground-based observations in the NCP and TW regions from January to December, respectively. The orange bars and green lines represent the monthly averaged AOD and relative humidity (RH). The RH data were obtained from the ECMWF ERA-Interim product.

It can be found that in the NCP region (first column), AHI AOD has the best performance in summer with the highest AOD levels, and it did the opposite in Taiwan, where the AOD level is the lowest in summer. The comparison further implies the impact of AOD levels on the accuracy of satellite-retrieved AOD. MERRA-2 shows a relatively stable performance in NCP, with the lowest accuracy in August, and it has a better performance in winter and early spring in TW. CAMS AOD exhibits similar seasonal variations to MERRA-2. By comparing the seasonal changes of RH, it can be found that the RH is high when the accuracy of AOD is low. Studies have shown that when RH is greater than 65%, the aerosol hygroscopic effect is significant [48], hence introducing the large bias in AOD retrievals. This interference is obviously more pronounced in TW due to the more hydrophilic sea-salt aerosols and higher humidity.

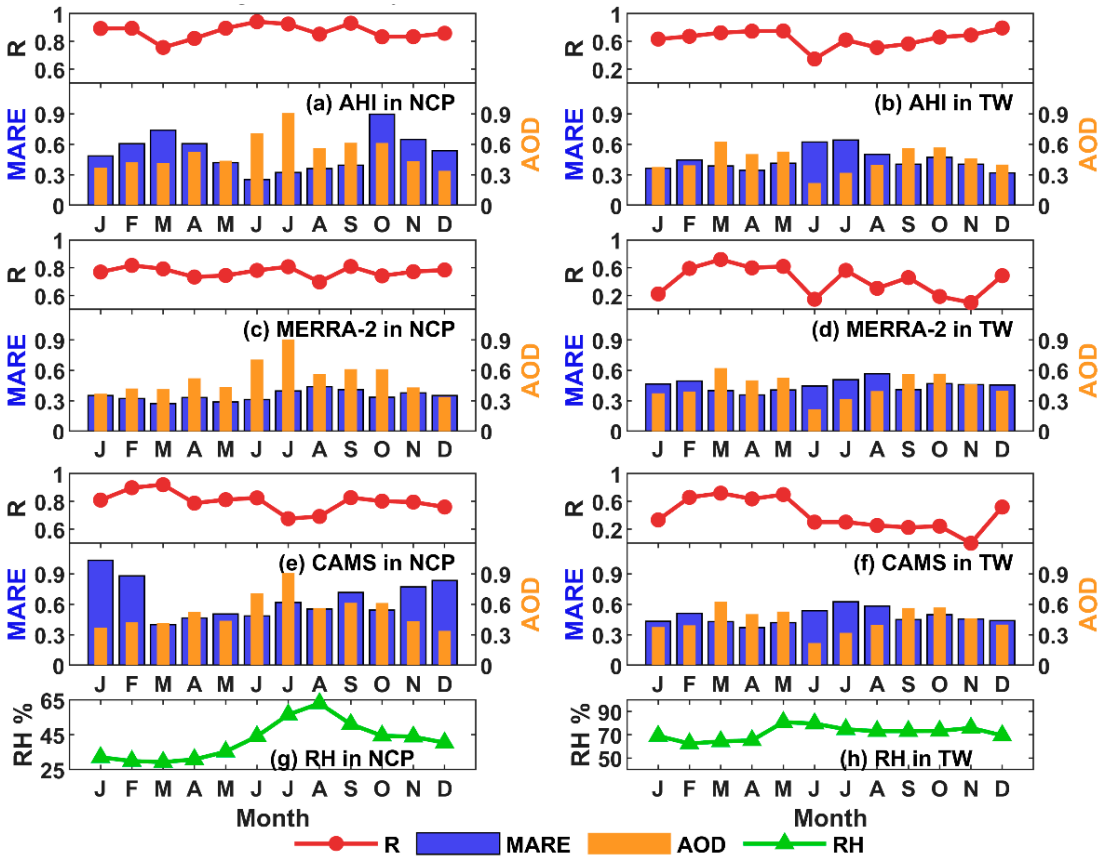

Figure 8. The seasonal cycle of R (red lines) and MARE (blue bars) between (**a**–**b**) AHI, (**c**–**d**) MERRA-2, and (**e**–**f**) CAMS AODs versus ground-based observations in the NCP and TW regions. Monthly AOD (orange bars) are averaged based on AERONET AOD 500 nm. Green line represents the monthly relative humidity (RH) levels near the surface.

4. Conclusions

With fast industrialization and development in China, the issue of aerosol pollution has drawn significant attention. Recent developments in aerosol-related research have shown that AOD as a fundamental property indicating aerosol loadings have increased the need for AOD data with a high spatio-temporal resolution [49,50]. Hourly/sub-daily AODs of the geostationary satellites and typical reanalysis products make it possible to capture diurnal variations of aerosol loadings. AHI AOD of version 030 shows notable improvements in comparison to the prior version. In this

study, the hourly AOD data provided by Himawari-8/AHI V030 L3 dataset were evaluated against AERONET measurements and then compared with two reanalysis AOD products from MERRA-2 and CAMS respectively, from July 2015 to December 2017 over China (see Table 2 for the validation statistics summary). AHI AOD shows the highest R value of 0.82, lowest RMSE of 0.23, and moderate MARE of 0.56, while MERRA-2 and CAMS AODs have lower R values (0.74, 0.72) and higher RMSE (0.28, 0.26). There is significant underestimation in the MERRA-2 product at the high AOD range. Missing nitrate aerosols in the reanalysis models might be an important contributing factor [16,31].

Table 2. Validation statistics of AOD products under different conditions.

		AHI V030			MERRA-2			CAMS		
		R	**RMSE**	**MARE**	**R**	**RMSE**	**MARE**	**R**	**RMSE**	**MARE**
All sites	All	0.82	0.23	0.56	0.74	0.28	0.39	0.72	0.26	0.62
	morning	0.89	0.22	0.39	0.70	0.30	0.41	0.74	0.27	0.60
	noon	0.84	0.23	0.70	0.79	0.28	0.40	0.75	0.26	0.66
	afternoon	0.77	0.24	0.53	0.69	0.25	0.35	0.61	0.27	0.58
NCP	All	0.87	0.22	0.55	0.79	0.29	0.34	0.81	0.26	0.66
	AOD ≤ 0.5	0.48	0.18	0.74	0.68	0.10	0.31	0.63	0.21	0.88
	AOD > 0.5	0.80	0.27	0.24	0.54	0.46	0.40	0.60	0.33	0.29
	AE ≤ 1	0.87	0.23	0.78	0.82	0.30	0.33	0.82	0.26	0.85
	AE > 1	0.88	0.21	0.47	0.77	0.28	0.35	0.80	0.26	0.59
HK	All	0.82	0.22	0.32	0.80	0.22	0.32	0.72	0.23	0.40
	AOD ≤ 0.5	0.50	0.12	0.34	0.53	0.10	0.34	0.46	0.13	0.47
	AOD > 0.5	0.74	0.32	0.29	0.66	0.33	0.30	0.60	0.34	0.30
TW	All	0.67	0.27	0.43	0.47	0.30	0.45	0.44	0.30	0.47
	AOD ≤ 0.5	0.44	0.15	0.46	0.45	0.11	0.44	0.44	0.11	0.46
	AOD > 0.5	0.42	0.40	0.37	0.15	0.47	0.47	0.13	0.48	0.49
	AE ≤ 1	0.69	0.44	0.70	0.47	0.54	0.71	0.36	0.56	0.83
	AE > 1	0.67	0.24	0.39	0.52	0.25	0.42	0.50	0.26	0.43
Baotou	All	0.59	0.17	0.69	0.77	0.07	0.37	0.59	0.13	0.68
	AE ≤ 1	0.57	0.17	0.72	0.84	0.06	0.30	0.58	0.18	0.92
	AE > 1	0.60	0.17	0.68	0.73	0.08	0.41	0.69	0.09	0.53
Taihu	All	0.75	0.23	0.39	0.67	0.21	0.34	0.83	0.26	0.65
	AOD ≤ 0.5	0.48	0.16	0.47	0.59	0.11	0.37	0.67	0.26	0.90
	AOD > 0.5	0.60	0.29	0.29	0.33	0.28	0.30	0.71	0.26	0.35
	AE ≤ 1	0.72	0.21	0.44	0.56	0.17	0.24	0.76	0.19	0.46
	AE > 1	0.75	0.23	0.38	0.67	0.21	0.35	0.84	0.26	0.66

The performance of AHI and reanalysis AOD datasets vary in different regions, which can be mainly ascribed to the different local pollution levels. In the NCP, HK, TW, and Taihu regions, AHI AOD shows better performance than MERRA-2 and CAMS AODs, and its accuracy could be improved with the increase of AOD levels. While in Baotou, MERRA-2 AOD shows the highest consistency with ground-based observations. It should be cautious to use AHI AOD in bright surface area. AHI product is reliable in regions with high aerosol pollution levels like the central and eastern China, while in the vast western or northwestern China, the MERRA-2 AOD product may be more suitable.

The accuracy of all three AOD products shows diurnal and seasonal variability. AHI AOD performs better in the morning, which might be mostly contributed by a higher AOD level. Reanalysis AODs have the best consistency with ground-based observations at noon due to the assimilated MODIS AOD from Aqua with higher accuracy than from Terra. AHI AOD illustrates better performance in summer in the NCP region, and MERRA-2 AOD can be considered proper surrogate-data during periods with low pollution levels like spring and autumn. All AOD datasets show lower accuracy in TW during summertime due to the low pollution levels and high RH conditions, accompanied by the weakly reliable surface reflectance assumption. The significant underestimation of reanalysis AODs in

TW should be mainly ascribed to the water-uptake by hydrophilic sea-salt aerosols under a relatively high humidity condition. AHI AOD is considered more reliable over the whole time in TW.

Overall, the comprehensive evaluation work between Himawari-8/AHI and reanalysis AOD products provides detailed guidance for choosing different aerosol data on different occasions. In the future, by involving more adequate ground-based observations, more accurate comparisons for the satellite and reanalysis aerosol products can be conducted.

Author Contributions: Conceptualization, F.M. and Y.W.; methodology, T.Z. and L.Z.; formal analysis, T.Z.; writing—original draft preparation, T.Z.; writing—review and editing, L.Z. and Y.Z. All authors have read and agreed to the published version of the manuscript.

Funding: This research was funded by the National Key Research and Development Program of China (grant number 2018YFD1100405, 2017YFC0212600) and the National Natural Science Foundation of China (grant number 41701381, 41971285).

Acknowledgments: The authors thank JAXA, ECMWF and NASA for providing the datasets used in this study.

Conflicts of Interest: The authors declare no conflict of interest.

References

1. Han, X.; Liu, Y.; Gao, H.; Ma, J.; Mao, X.; Wang, Y.; Ma, X. Forecasting PM2. 5 induced male lung cancer morbidity in China using satellite retrieved PM2. 5 and spatial analysis. *Sci. Total Environ.* **2017**, *607*, 1009–1017. [CrossRef] [PubMed]
2. Pope, C.A., III; Burnett, R.T.; Turner, M.C.; Cohen, A.; Krewski, D.; Jerrett, M.; Gapstur, S.M.; Thun, M.J. Lung cancer and cardiovascular disease mortality associated with ambient air pollution and cigarette smoke: Shape of the exposure-response relationships. *Environ. Health Perspect.* **2011**, *119*, 1616–1621. [CrossRef] [PubMed]
3. Stocker, T.F.; Qin, D.; Plattner, G.-K.; Tignor, M.; Allen, S.K.; Boschung, J.; Nauels, A.; Xia, Y.; Bex, V.; Midgley, P.M. *IPCC, 2013: Climate Change 2013: The Physical Science Basis*; Stocker, T.F., Qin, D., Plattner, G.-K., Tignor, M., Allen, S.K., Boschung, J., Nauels, A., Xia, Y., Bex, V., Midgley, P.M., Eds.; Cambridge University Press: Cambridge, UK; New York, NY, USA, 2013.
4. Wang, J.; Christopher, S.A. Intercomparison between satellite-derived aerosol optical thickness and PM2.5 mass: Implications for air quality studies. *Geophys. Res. Lett.* **2003**, *30*, 2095. [CrossRef]
5. Waquet, F.; Riedi, J.; Labonnote, L.C.; Goloub, P.; Cairns, B.; Deuzé, J.L.; Tanré, D. Aerosol remote sensing over clouds using A-Train observations. *J. Atmos. Sci.* **2009**, *66*, 2468–2480. [CrossRef]
6. Daisaku, U. Aerosol optical depth product derived from Himawari-8 data for Asian dust monitoring. *Meteorol. Satell. Cent. Tech. Note* **2016**, *16*, 56–63.
7. Bessho, K.; Date, K.; Hayashi, M.; Ikeda, A.; Imai, T.; Inoue, H.; Kumagai, Y.; Miyakawa, T.; Murata, H.; Ohno, T. An introduction to Himawari-8/9—Japan's new-generation geostationary meteorological satellites. *J. Meteorol. Soc. Jpn. Ser. II* **2016**, *94*, 151–183. [CrossRef]
8. Zhang, Z.; Wu, W.; Fan, M.; Tao, M.; Wei, J.; Jin, J.; Tan, Y.; Wang, Q. Validation of Himawari-8 aerosol optical depth retrievals over China. *Atmos. Environ.* **2019**, *199*, 32–44. [CrossRef]
9. Wang, W.; Mao, F.; Pan, Z.; Gong, W.; Yoshida, M.; Zou, B.; Ma, H. Evaluating aerosol optical depth from Himawari-8 with sun photometer network. *J. Geophys. Research: Atmos.* **2019**, *124*, 5516–5538. [CrossRef]
10. Rienecker, M.M.; Suarez, M.J.; Gelaro, R.; Todling, R.; Bacmeister, J.; Liu, E.; Bosilovich, M.G.; Schubert, S.D.; Takacs, L.; Kim, G.-K. MERRA: NASA's modern-era retrospective analysis for research and applications. *J. Clim.* **2011**, *24*, 3624–3648. [CrossRef]
11. Lynch, P.; Reid, J.S.; Westphal, D.L.; Zhang, J.; Hogan, T.F.; Hyer, E.J.; Curtis, C.A.; Hegg, D.A.; Shi, Y.; Campbell, J.R. An 11-year global gridded aerosol optical thickness reanalysis (v1. 0) for atmospheric and climate sciences. *Geosci. Model Dev.* **2016**, *9*, 1489–1522. [CrossRef]
12. Georgoulias, A.K.; Tsikerdekis, A.; Amiridis, V.; Marinou, E.; Benedetti, A.; Zanis, P.; Alexandri, G.; Kourtidis, K.; Lelieveld, J. Evaluation of the MACC reanalysis dust product over Europe, Northern Africa and Middle East using CALIOP/CALIPSO satellite observations. In Proceedings of the EGU General Assembly Conference Abstracts (EGU2018), Vienna, Austria, 4–13 April 2018; p. 17050.

13. Randles, C.A.; Da Silva, A.M.; Buchard, V.; Colarco, P.R.; Darmenov, A.; Govindaraju, R.; Smirnov, A.; Holben, B.; Ferrare, R.; Hair, J. The MERRA-2 aerosol reanalysis, 1980 onward. Part I: System description and data assimilation evaluation. *J. Clim.* **2017**, *30*, 6823–6850. [CrossRef] [PubMed]
14. Inness, A.; Ades, M.; Agusti-Panareda, A.; Barré, J.; Benedictow, A.; Blechschmidt, A.-M.; Dominguez, J.; Engelen, R.; Eskes, H.; Flemming, J.; et al. The CAMS reanalysis of atmospheric composition. *Atmos. Chem. Phys.* **2019**, *19*, 3515–3556. [CrossRef]
15. Shi, H.; Xiao, Z.; Zhan, X.; Ma, H.; Tian, X. Evaluation of MODIS and two reanalysis aerosol optical depth products over AERONET sites. *Atmos. Res.* **2019**, *220*, 75–80. [CrossRef]
16. Buchard, V.; Randles, C.A.; Da Silva, A.M.; Darmenov, A.; Colarco, P.R.; Govindaraju, R.; Ferrare, R.; Hair, J.; Beyersdorf, A.J.; Ziemba, L.D. The MERRA-2 aerosol reanalysis, 1980 onward. Part II: Evaluation and case studies. *J. Clim.* **2017**, *30*, 6851–6872. [CrossRef]
17. Zhang, X.; Wang, L.; Wang, W.; Cao, D.; Wang, X.; Ye, D. Long-term trend and spatiotemporal variations of haze over China by satellite observations from 1979 to 2013. *Atmos. Environ.* **2015**, *119*, 362–373. [CrossRef]
18. Yumimoto, K.; Nagao, T.M.; Kikuchi, M.; Sekiyama, T.T.; Murakami, H.; Tanaka, T.Y.; Ogi, A.; Irie, H.; Khatri, P.; Okumura, H. Aerosol data assimilation using data from Himawari-8, a next-generation geostationary meteorological satellite. *Geophys. Res. Lett.* **2016**, *43*, 5886–5894. [CrossRef]
19. Kikuchi, M.; Murakami, H.; Suzuki, K.; Nagao, T.M.; Higurashi, A. Improved hourly estimates of aerosol optical thickness using spatiotemporal variability derived from Himawari-8 geostationary satellite. *IEEE Trans. Geosci. Remote Sens.* **2018**, *56*, 3442–3455. [CrossRef]
20. Omar, A.H.; Won, J.G.; Winker, D.M.; Yoon, S.C.; Dubovik, O.; McCormick, M.P. Development of global aerosol models using cluster analysis of Aerosol Robotic Network (AERONET) measurements. *J. Geophys. Res. Atmos.* **2005**, *110*, D10S14. [CrossRef]
21. Sayer, A.M.; Smirnov, A.; Hsu, N.C.; Holben, B.N. A pure marine aerosol model, for use in remote sensing applications. *J. Geophys. Res. Atmos.* **2012**, *117*, D05213. [CrossRef]
22. Fukuda, S.; Nakajima, T.; Takenaka, H.; Higurashi, A.; Kikuchi, N.; Nakajima, T.Y.; Ishida, H. New approaches to removing cloud shadows and evaluating the 380 nm surface reflectance for improved aerosol optical thickness retrievals from the GOSAT/TANSO-Cloud and Aerosol Imager. *J. Geophys. Res. Atmos.* **2013**, *118*, 13520–513531. [CrossRef]
23. Yarwood, G.; Rao, S.; Yocke, M.; Whitten, G. Updates to the Carbon Bond Chemical MEchanism: CB05. Final report to the US EPA, EPA Report Number: RT-0400675. December 2005. Available online: http://www.camx.com (accessed on 20 February 2020).
24. Giles, D.M.; Sinyuk, A.; Sorokin, M.G.; Schafer, J.S.; Smirnov, A.; Slutsker, I.; Eck, T.F.; Holben, B.N.; Lewis, J.R.; Campbell, J.R. Advancements in the Aerosol Robotic Network (AERONET) Version 3 database—automated near-real-time quality control algorithm with improved cloud screening for Sun photometer aerosol optical depth (AOD) measurements. *Atmos. Measurement Tech.* **2019**, *12*, 169–209. [CrossRef]
25. Huang, J.; Kondragunta, S.; Laszlo, I.; Liu, H.; Remer, L.A.; Zhang, H.; Superczynski, S.; Ciren, P.; Holben, B.N.; Petrenko, M. Validation and expected error estimation of Suomi-NPP VIIRS aerosol optical thickness and Ångström exponent with AERONET. *J. Geophys. Rese. Atmos.* **2016**, *121*, 7139–7160. [CrossRef]
26. Eck, T.F.; Holben, B.; Reid, J.; Dubovik, O.; Smirnov, A.; O'neill, N.; Slutsker, I.; Kinne, S. Wavelength dependence of the optical depth of biomass burning, urban, and desert dust aerosols. *J. Geophys. Res.Atmos.* **1999**, *104*, 31333–31349. [CrossRef]
27. Kahn, R.A.; Gaitley, B.J.; Garay, M.J.; Diner, D.J.; Eck, T.F.; Smirnov, A.; Holben, B.N. Multiangle Imaging SpectroRadiometer global aerosol product assessment by comparison with the Aerosol Robotic Network. *J. Geophys. Res. Atmos.* **2010**, *115*, D23209. [CrossRef]
28. Gillard, J.W. *An historical overview of linear regression with errors in both variables*; Technical Report; Cardiff University: Cardiff, UK, 2006.
29. Wu, C.; Yu, J. Evaluation of linear regression techniques for atmospheric applications: The importance of appropriate weighting. *Atmos. Measurement Tech. Discuss.* **2017**, 1–31. [CrossRef]
30. Flemming, J.; Benedetti, A.; Inness, A.; Engelen, R.J.; Jones, L.; Huijnen, V.; Remy, S.; Parrington, M.; Suttie, M.; Bozzo, A. The CAMS interim reanalysis of carbon monoxide, ozone and aerosol for 2003–2015. *Atmos. Chem. Phys.* **2017**, *17*, 1945–1983. [CrossRef]

31. Buchard, V.; Da Silva, A.M.; Randles, C.A.; Colarco, P.; Ferrare, R.; Hair, J.; Hostetler, C.; Tackett, J.; Winker, D. Evaluation of the surface PM2.5 in Version 1 of the NASA MERRA Aerosol Reanalysis over the United States. *Atmos. Environ.* **2016**, *125*, 100–111. [CrossRef]
32. Wei, J.; Li, Z.; Sun, L.; Peng, Y.; Zhang, Z.; Li, Z.; Su, T.; Feng, L.; Cai, Z.; Wu, H. Evaluation and uncertainty estimate of next-generation geostationary meteorological Himawari-8/AHI aerosol products. *Sci. Total Environ.* **2019**, *692*, 879–891. [CrossRef]
33. Wang, L.; Xin, J.; Wang, Y.; Li, Z.; Liu, G.; Li, J. Evaluation of the MODIS aerosol optical depth retrieval over different ecosystems in China during EAST-AIRE. *Atmos. Environ.* **2007**, *41*, 7138–7149. [CrossRef]
34. Zhang, W.; Xu, H.; Zhang, L. Assessment of Himawari-8 AHI Aerosol Optical Depth Over Land. *Remote Sens.* **2019**, *11*, 1108. [CrossRef]
35. Ahn, C.; Torres, O.; Bhartia, P.K. Comparison of ozone monitoring instrument UV aerosol products with Aqua/Moderate Resolution Imaging Spectroradiometer and Multiangle Imaging Spectroradiometer observations in 2006. *J. Geophys. Res. Atmos.* **2008**, *113*, 1–13. [CrossRef]
36. Zhang, W.; Gu, X.; Xu, H.; Yu, T.; Zheng, F. Assessment of OMI near-UV aerosol optical depth over Central and East Asia. *J. Geophys. Res. Atmos.* **2016**, *121*, 382–398. [CrossRef]
37. Rupakheti, D.; Kang, S.; Rupakheti, M.; Cong, Z.; Panday, A.K.; Holben, B.N. Identification of absorbing aerosol types at a site in the northern edge of Indo-Gangetic Plain and a polluted valley in the foothills of the central Himalayas. *Atmos. Res.* **2019**, *223*, 15–23. [CrossRef]
38. Schuster, G.L.; Dubovik, O.; Holben, B.N. Angstrom exponent and bimodal aerosol size distributions. *J. Geophys. Res.* **2006**, *111*, D07207. [CrossRef]
39. Kaskaoutis, D.G.; Kambezidis, H.D.; Hatzianastassiou, N.; Kosmopoulos, P.G.; Badarinath, K. Aerosol climatology: On the discrimination of aerosol types over four AERONET sites. *Atmos. Chem. Phys. Discuss.* **2007**, *7*, 6357–6411. [CrossRef]
40. Chan, K.L. Aerosol optical depths and their contributing sources in Taiwan. *Atmos. Environ.* **2017**, *148*, 364–375. [CrossRef]
41. Grythe, H.; Ström, J.; Krejci, R.; Quinn, P.; Stohl, A. A review of sea-spray aerosol source functions using a large global set of sea salt aerosol concentration measurements. *Atmos. Chem. Phys.* **2014**, *14*, 1277–1297. [CrossRef]
42. Fei, K.-C.; Wu, L.; Zeng, Q.-C. Aerosol optical depth and burden from large sea salt particles. *J. Geophys. Res. Atmos.* **2018**, *124*, 1680–1696. [CrossRef]
43. Wang, H.; Wang, Q.; Chen, J.; Chen, C.; Huang, C.; Qiao, L.; Lou, S.; Lu, J. Do vehicular emissions dominate the source of C6-C8 aromatics in the megacity Shanghai of eastern China? *J. Environ. Sci.* **2015**, *27*, 290–297. [CrossRef]
44. Beyersdorf, A.J.; Ziemba, L.D.; Chen, G.; Corr, C.A.; Crawford, J.H.; Diskin, G.S.; Moore, R.H.; Thornhill, K.L.; Winstead, E.L.; Anderson, B.E. The impacts of aerosol loading, composition, and water uptake on aerosol extinction variability in the Baltimore-Washington, DC region. *Atmos. Chem. Phys.* **2016**, *16*, 1003–1015. [CrossRef]
45. Bright, J.M.; Gueymard, C.A. Climate-specific and global validation of MODIS Aqua and Terra aerosol optical depth at 452 AERONET stations. *Sol. Energ.* **2019**, *183*, 594–605. [CrossRef]
46. Jiang, T.; Chen, B.; Chan, K.K.Y.; Xu, B. Himawari-8/AHI and MODIS Aerosol Optical Depths in China: Evaluation and Comparison. *Remote Sens.* **2019**, *11*, 1011. [CrossRef]
47. Zhang, T.; Zang, L.; Wan, Y.; Wang, W.; Zhang, Y. Ground-level PM2.5 estimation over urban agglomerations in China with high spatiotemporal resolution based on Himawari-8. *Sci. Total Environ.* **2019**, *676*, 535–544. [CrossRef]
48. Zang, L.; Wang, Z.; Zhu, B.; Zhang, Y. Roles of Relative Humidity in Aerosol Pollution Aggravation over Central China during Wintertime. *Int. J. Environ. Res. Pub. Health* **2019**, *16*, 4422. [CrossRef]
49. Wei, J.; Peng, Y.; Sun, L.; Guo, J. Intercomparison in spatial distributions and temporal trends derived from multi-source satellite aerosol products. *Atmos. Chem. Phys.* **2019**, *19*, 7183–7207. [CrossRef]
50. Pan, Z.; Mao, F.; Wang, W.; Zhu, B.; Lu, X.; Gong, W. Impacts of 3D aerosol, cloud, and water vapor variations on the recent brightening during the South Asian monsoon season. *Remote Sens.* **2018**, *10*, 651. [CrossRef]